J|A|C|S
ARTICLES

Published on Web 02/02/2010

Monitoring Self-Sorting by Electrospray Ionization Mass Spectrometry: Formation Intermediates and Error-Correction during the Self-Assembly of Multiply Threaded Pseudorotaxanes

Wei Jiang, Andreas Schäfer, Parveen Choudhary Mohr, and Christoph A. Schalley*

Institut für Chemie und Biochemie, Freie Universität Berlin, Takustrasse 3, 14195 Berlin, Germany

Received December 1, 2009; E-mail: christoph@schalley-lab.de

Abstract: Three binary pseudorotaxanes, which are based on two different secondary ammonium/crown ether binding motifs, have been studied by ^{1}H NMR and ^{1}H,^{1}H EXSY NMR experiments with respect to their thermodynamic stabilities and their axle exchange kinetics. The stability ranking does not follow the order of axle exchange rates, and the thermodynamically most stable axle−wheel combinations assemble only slowly. On the basis of these binding motifs, a series of self-sorting systems have been studied ranging from simple four-component mixtures through sequence-specific pseudorotaxanes to multiply threaded complexes. Because of the mismatch of kinetic and thermodynamic order, wrongly assembled structures are unavoidable, which require error-correction steps to yield the final thermodynamically controlled self-sorted products. These error-correction steps can easily be monitored by electrospray mass spectrometry, when a mixed-flow microreactor is coupled to the ion source to cover second time scales. Self-assembly intermediates, wrongly assembled structures, and the final thermodynamic products can be simultaneously identified. The determination of preferred assembly pathways as well as the formation of dead-end structures provides a clear picture of a rich kinetic behavior of the self-sorting systems under study.

Introduction

Self-assembly[1] has attracted great attention in the last two decades due to its vital importance in biological systems and its application in a "bottom-up" approach for the construction of nano- and soft materials[2] or molecular machines and devices.[3] The maturity of this field has been marked by the successful constructions of many spectacular supramolecular aggregates with increasing complexity, such as cyclic rosettes,[4] self-assembled capsules,[5] metallo-supramolecular polygons and polyhedrons,[6] trefoil knots,[7] and Borromean rings.[8] In particular, multicomponent self-assembly is highly efficient for achieving giant supramolecular architectures by incorporating many small building blocks through noncovalent interactions. The repetitive use of the same building blocks has the advantage that the instructions written to the molecules are very simple, and thus their synthesis is often quite easy to accomplish. However, the price is that the resulting supramolecular aggregates are often functionally limited by their highly symmetrical structures.

(1) (a) Whitesides, G. M.; Mathias, J. P.; Seto, C. T. *Science* **1991**, *254*, 1312–1319. (b) Lindsey, J. S. *New J. Chem.* **1991**, *15*, 153–180. (c) Philp, D.; Stoddart, J. F. *Angew. Chem.* **1996**, *108*, 1242–1286; *Angew Chem., Int. Ed. Engl*. **1996**, *35*, 1154−1196. (d) Whitesides, G. M.; Grzybowski, B. *Science* **2002**, *295*, 2418–2421. (e) Schalley, C. A.; Lützen, A.; Albrecht, M. *Chem.-Eur. J.* **2004**, *10*, 1072–1080.

(2) For several reviews: (a) Hamley, I. W. *Angew. Chem.* **2003**, *115*, 1730–1752; *Angew Chem., Int. Ed*. **2003**, *42*, 1692−1712. (b) Katz, E.; Willner, I. *Angew. Chem.* **2004**, *116*, 6166–6235; *Angew. Chem., Int. Ed*. **2004**, *43*, 6042−6108. (c) Love, J. C.; Estroff, L. A.; Kriebel, J. K.; Nuzzo, R. G.; Whitesides, G. M. *Chem. Rev.* **2005**, *105*, 1103–1170. (d) Vemula, P. K.; John, G. *Acc. Chem. Res.* **2008**, *41*, 769–782.

(3) Selected books and reviews: (a) Balzani, V.; Credi, A.; Raymo, F. M.; Stoddart, J. F. *Angew. Chem.* **2000**, *112*, 3438–3530; *Angew. Chem., Int. Ed*. **2000**, *39*, 3348−3391. (b) *Molecular Switches*; Feringa, B. L., Ed.; Wiley-VCH: Weinheim, Germany, 2001. (c) Balzani, V.; Venturi, M.; Credi, A. *Molecular Devices and Machines*; Wiley-VCH: Weinheim, Germany, 2003. (d) Kay, E. R.; Leigh, D. A.; Zerbetto, F. *Angew. Chem.* **2007**, *119*, 72–196; *Angew. Chem., Int. Ed*. **2007**, *46*, 72−191. (e) Balzani, V. *Pure Appl. Chem.* **2008**, *80*, 1631–1650.

(4) (a) Whitesides, G. M.; Simanek, E. E.; Mathias, J. P.; Seto, C. T.; Chin, D. N.; Mammen, M.; Gordon, D. M. *Acc. Chem. Res.* **1995**, *28*, 37–44, and references thereinTwo more examples: (b) Marsh, A.; Silvestri, M.; Lehn, J.-M. *Chem. Commun.* **1996**, 1527–1528. (c) Vreekamp, R. H.; John, P. M.; van Duynhoven, J. P. M.; Hubert, M.; Verhoom, W.; Reinhoudt, D. N. *Angew. Chem.* **1996**, *108*, 1306–1309; *Angew. Chem., Int. Ed. Engl*. **1996**, *35*, 1218−1235.

(5) (a) Conn, M. M.; Rebek, J., Jr. *Chem. Rev.* **1997**, *97*, 1647–1668. (b) Hof, F.; Craig, S. L.; Nuckolls, C.; Rebek, J., Jr. *Angew. Chem.* **2002**, *114*, 1556–1578; *Angew. Chem., Int. Ed*. **2002**, *41*, 1488−1508. (c) Biros, S. M.; Rebek, J., Jr. *Chem. Soc. Rev.* **2007**, *36*, 93–104, and references therein.

(6) Selected reviews: (a) Fujita, M. *Acc. Chem. Res.* **1999**, *32*, 53–61. (b) Leininger, S.; Olenyuk, B.; Stang, P. J. *Chem. Rev.* **2000**, *100*, 853–908. (c) Albrecht, M. *Chem. Rev.* **2001**, *101*, 3457–3498. (d) Seidel, S. R.; Stang, P. J. *Acc. Chem. Res.* **2002**, *35*, 972–983. (e) Würthner, F.; You, C.-C.; Saha-Möller, C. *Chem. Soc. Rev.* **2004**, *33*, 133–146. (f) Ruben, M.; Rojo, J.; Romero-Salguero, F. J.; Uppadine, L. H.; Lehn, J.-M. *Angew. Chem.* **2004**, *116*, 3728–3747; *Angew. Chem., Int. Ed*. **2004**, *43*, 3644−3662. (g) You, C.-C.; Dobrawa, R.; Saha-Möller, C.; Würthner, F. *Top. Curr. Chem.* **2005**, *258*, 39–82. (h) Fujita, M.; Tominaga, M.; Hori, A.; Therrien, B. *Acc. Chem. Res.* **2005**, *38*, 371–380. (i) Li, S.-S.; Northrop, B. H.; Yuan, Q.-H.; Wan, L.-J.; Stang, P. J. *Acc. Chem. Res.* **2009**, *42*, 249–259.

(7) (a) Dietrich-Buchecker, C. O.; Sauvage, J.-P. *Angew. Chem.* **1989**, *101*, 192–194; *Angew. Chem., Int. Ed. Engl*. **1989**, *28*, 189−192. (b) Safarowsky, O.; Neiger, M.; Fröhlich, R.; Vögtle, F. *Angew. Chem.* **2000**, *112*, 1699–1701; *Angew. Chem., Int. Ed*. **2000**, *39*, 1616−1618.

Recently, molecular networks[9] composed of many different molecules have been introduced to increase the complexity[10] of chemical systems and further to achieve more complex function. Among them, self-sorting systems[11,12] are more organized because they select only one or a few complexes out of a larger number of potentially possible assemblies. Nevertheless, simple self-sorting systems will still lead to mixtures of several discrete assemblies. In contrast, the integrative self-sorting systems,[12] which combine the advantages of self-assembly and self-sorting, integrate all distinct components into one well-defined assembly with precise positional control. This strategy enhances the structural complexity and diversity of synthetic supramolecular architectures and thus lays the structural basis for the implementation of complex function in future assemblies.

Electrospray mass spectrometry (ESI-MS)[13] is able to detect many different species simultaneously and thus provides at least qualitative information on complex mixtures. It has, for example, been applied to the investigation of complex chemical systems, such as the formation dynamics of inorganic clusters.[14] This soft ionization method has also been widely applied to the characterization of supramolecules.[15,16] Although the kinetics of many binary supramolecular systems have been well studied,[17] the studies on multicomponent systems[18,19] are relatively rare. In multicomponent systems, many species, including the free components, reaction intermediates, wrongly assembled structures, and the desired final thermodynamic assemblies, coexist in varying concentrations until equilibrium is reached. ESI-MS is capable of resolving such complex mixtures and of monitoring the dynamic processes of complex supramolecular systems.[19] Thus, it could facilitate the discovery of self-assembly intermediates and dead-end structures, which need to reassemble into the correct structures. In addition, by coupling to a mixed-flow microreactor, the time window detectable by ESI-MS can

(8) (a) Chichak, K. S.; Cantrill, S. J.; Pease, A. R.; Chiu, S.-H.; Cave, G. W. V.; Atwood, J. L.; Stoddart, J. F. *Science* **2004**, *304*, 1308–1312. A review on this topic: (b) Cantrill, S. J.; Chichak, K. S.; Peters, A. J.; Stoddart, J. F. *Acc. Chem. Res.* **2005**, *38*, 1–9.

(9) For a review: (a) Corbett, P. T.; Leclaire, J.; Vial, L.; West, K. R.; Wietor, J.-L.; Sanders, J. K. M.; Otto, S. *Chem. Rev.* **2006**, *106*, 3652–3711. (b) Nitschke, J. R. *Acc. Chem. Res.* **2007**, *40*, 103–112. (c) Ludlow, R. F.; Otto, S. *Chem. Soc. Rev.* **2008**, *37*, 101–108. (d) Northrop, B. H.; Zheng, Y.-R.; Chi, K.-W.; Stang, P. J. *Acc. Chem. Res.* **2009**, *42*, 1554–1563.

(10) (a) Lehn, J.-M. *Science* **2002**, *295*, 2400–2403. (b) Lehn, J.-M. *Proc. Natl. Acad. Sci. U.S.A.* **2002**, *99*, 4763–4768. (c) Service, R. F. *Science* **2005**, *309*, 95. (d) Lehn, J.-M. *Chem. Soc. Rev.* **2007**, *36*, 151–160. (e) Schmittel, M.; Mahata, K. *Angew. Chem.* **2008**, *120*, 5364–5366; *Angew. Chem., Int. Ed.* **2008**, *47*, 5284−5286. (f) Stoddart, J. F. *Nat. Chem.* **2009**, *1*, 14–15. (g) Gibb, B. C. *Nat. Chem.* **2009**, *1*, 17–18.

(11) For selected examples, see: (a) Wu, A.-X.; Isaacs, L. *J. Am. Chem. Soc.* **2003**, *125*, 4831–4835. (b) Mukhopadhyay, P.; Wu, A.-X.; Isaacs, L. *J. Org. Chem.* **2004**, *69*, 6157–6164. (c) Liu, S.-M.; Ruspic, C.; Mukhopadhyay, P.; Chakrabarti, S.; Zavalij, P. Y.; Isaacs, L. *J. Am. Chem. Soc.* **2005**, *127*, 15959–15967. (d) Chakrabarti, S.; Mukhopadhyay, P.; Lin, S.; Isaacs, L. *Org. Lett.* **2007**, *9*, 2349–2352. (e) Ghosh, S.; Wu, A.-X.; Fettinger, J. C.; Zavalij, P. Y.; Isaacs, L. *J. Org. Chem.* **2008**, *73*, 5915–5925. (f) Braekers, D.; Peters, C.; Bogdan, A.; Rudzevich, Y.; Böhmer, V.; Desreux, J. F. *J. Org. Chem.* **2008**, *73*, 701–706. (g) Rudzevich, Y.; Rudzevich, V.; Klautzsch, F.; Schalley, C. A.; Böhmer, V. *Angew. Chem.* **2009**, *121*, 3925–3929; *Angew. Chem., Int. Ed.* **2009**, *48*, 3867−3871. (h) Rekharsky, M. V.; Yamamura, H.; Ko, Y. H.; Selvapalam, N.; Kim, K.; Inoue, Y. *Chem. Commun.* **2008**, 2236–2238. (i) Lin, J.-B.; Xu, X.-N.; Jiang, X.-K.; Li, Z.-T. *J. Org. Chem.* **2008**, *130*, 9403–9410. (j) Wang, F.; Han, C.-Y.; He, C.-L.; Zhou, Q.-Z.; Zhang, J.-Q.; Wang, C.; Li, N.; Huang, F.-H. *J. Am. Chem. Soc.* **2008**, *130*, 4375–4377. (k) Wang, F.; Zheng, B.; Zhu, K.-L.; Zhou, Q.-Z.; Zhai, C.-X.; Li, S.-J.; Li, N.; Huang, F.-H. *Chem. Commun.* **2009**, 2236–2238. (l) Barrett, E. S.; Dale, T. J.; Rebek, J., Jr. *J. Am. Chem. Soc.* **2008**, *130*, 2344–2350. (m) Ajami, D.; Hou, J.-L.; Dale, T. J.; Barrett, E.; Rebek, J., Jr. *Proc. Natl. Acad. Sci. U.S.A.* **2009**, *106*, 10430–10434. (n) Sugiyasu, K.; Kawano, S.; Fujita, N.; Shinkai, S. *Chem. Mater.* **2008**, *20*, 2863–2865. (o) Northrop, B. H.; Yang, H.-B.; Stang, P. J. *Inorg. Chem.* **2008**, 11257–11268. (p) Ito, H.; Furusho, Y.; Hasegawa, T.; Yashima, E. *J. Am. Chem. Soc.* **2009**, *130*, 14008–14015. (q) Tomimasu, N.; Kanaya, A.; Takashima, Y.; Yamaguchi, H.; Harada, A. *J. Am. Chem. Soc.* **2009**, *131*, 12339–12343. (r) Schmittel, M.; Mahata, K. *J. Am. Chem. Soc.* **2009**, *131*, 16544–16554.

(12) (a) Jiang, W.; Winkler, H. D. F.; Schalley, C. A. *J. Am. Chem. Soc.* **2008**, *130*, 13852–13853. (b) Jiang, W.; Schalley, C. A. *Proc. Natl. Acad. Sci. U.S.A.* **2009**, *106*, 10425–10429.

(13) Fenn, J. B. *Angew. Chem.* **2003**, *115*, 3999–4024; *Angew. Chem., Int. Ed.* **2003**, *42*, 3871−3894.

(14) (a) Bussian, P.; Sobott, F.; Brutschy, B.; Schrader, W.; Schüth, F. *Angew. Chem.* **2000**, *112*, 4065–4069; *Angew. Chem., Int. Ed.* **2000**, *39*, 3901−3905. (b) Pelster, S. A.; Schrader, W.; Schüth, F. *J. Am. Chem. Soc.* **2006**, *128*, 4310–4317. (c) Pester, S. A.; Kalamajka, R.; Schrader, W.; Schüth, F. *Angew. Chem.* **2007**, *119*, 2349–2352; *Angew. Chem., Int. Ed.* **2007**, *46*, 2299−2302. (d) Pester, S. A.; Weimann, B.; Schaack, B. B.; Schrader, W.; Schüth, F. *Angew. Chem.* **2007**, *119*, 6794–6797; *Angew. Chem., Int. Ed.* **2007**, *46*, 6674−6677. (e) Schaack, B. B.; Schrader, W.; Schüth, F. *Chem.-Eur. J.* **2009**, *15*, 5920–5925. (f) Schaack, B. B.; Schrader, W.; Corma, A.; Schüth, F. *Chem. Mater.* **2009**, *21*, 4448–4453. (g) Wilson, E. F.; Abbas, H.; Duncombe, B. J.; Streb, C.; Long, D.-L.; Cronin, L. *J. Am. Chem. Soc.* **2008**, *130*, 13876–13884. (h) Dharmaratne, A. C.; Krick, T.; Dass, A. *J. Am. Chem. Soc.* **2009**, *131*, 13604–13605.

(15) Reviews and book on the MS analysis of supramolecule: (a) Schalley, C. A. *Int. J. Mass Spectrom.* **2000**, *194*, 477–493. (b) Schalley, C. A. *Mass Spectrom. Rev.* **2001**, *20*, 253–309. (c) Baytekin, B.; Baytekin, H. T.; Schalley, C. A. *Org. Biomol. Chem.* **2006**, *4*, 2825–2841. (d) Miras, H. N.; Wilson, E. F.; Cronin, L. *Chem. Commun.* **2009**, 1297–1311. (e) Schalley, C. A.; Springer, A. *Mass Spectrometry and Gas-Phase Chemistry of Non-Covalent Complexes*; Wiley: Hoboken/USA, 2009.

(16) For some examples from very recent literature: (a) Zhang, H.-Z.; Grabenauer, M.; Bowers, M. T.; Dearden, D. V. *J. Phys. Chem. A* **2009**, *113*, 1508–1517. (b) Dearden, D. V.; Ferrell, T. A.; Asplund, M. C.; Zilch, L. W.; Julian, R. R.; Jarrold, M. F. *J. Phys. Chem. A* **2009**, *113*, 989–997. (c) Becherer, T.; Meshcheryakov, D.; Springer, A.; Böhmer, V.; Schalley, C. A. *J. Mass Spectrom.* **2009**, *44*, 1338–1347. (d) Au-Yeung, H. Y.; Pantos, G. D.; Sanders, J. K. M. *Proc. Natl. Acad. Sci. U.S.A.* **2009**, *106*, 10466–10470. (e) Albrecht, M.; Liu, Y.; Zhu, S. S.; Schalley, C. A.; Fröhlich, R. *Chem. Commun.* **2009**, 1195–1197. (f) Pierce, S. E.; Wang, J. M.; Jayawickramarajah, J.; Hamilton, A. D.; Brodbelt, J. S. *Chem.-Eur. J.* **2009**, *15*, 11244–11255. (g) Yang, H.-B.; Northrop, B. H.; Zheng, Y.-R.; Ghosh, K.; Stang, P. J. *J. Org. Chem.* **2009**, *74*, 7067–7074. (h) Zheng, Y.-R.; Northrop, B. H.; Yang, H.-B.; Zhao, L.; Stang, P. J. *J. Org. Chem.* **2009**, *74*, 3554–3557. (i) Janssen, P. G. A.; van Dongen, J. L. J.; Meijer, E. W.; Schenning, A. P. H. J. *Chem.-Eur. J.* **2009**, *15*, 352–360. (j) Han, Y.-T.; Li, X.-P.; Soler, M.; Wang, J.-L.; Wesdemiotis, C.; Newkome, G. R. *J. Am. Chem. Soc.* **2009**, *131*, 16395–16397.

(17) For selected examples, see: (a) Williams, A. R.; Northrop, B. H.; Houk, K. N.; Stoddart, J. F.; Williams, D. J. *Chem.-Eur. J.* **2004**, *10*, 5406–5421. (b) Badjić, J. D.; Cantrill, S. J.; Stoddart, J. F. *J. Am. Chem. Soc.* **2004**, *126*, 2288–2289. (c) Ashton, P. R.; Baxter, I.; Fyfe, M. C. T.; Raymo, F. M.; Spencer, N.; Stoddart, J. F.; White, A. J. P.; Williams, D. J. *J. Am. Chem. Soc.* **1998**, *120*, 2297–2307. (d) Marquez, C.; Nau, W. M. *Angew. Chem.* **2001**, *113*, 3248–3254; *Angew. Chem., Int. Ed.* **2001**, *40*, 3155−3160. (e) Marquez, C.; Hudgins, R. R.; Nau, W. M. *J. Am. Chem. Soc.* **2004**, *126*, 5806–5816. (f) Deutman, A. B. C.; Monnereau, C.; Elemans, J. A. A. W.; Ercolani, G.; Nolte, R. J. M.; Rowan, A. E. *Science* **2008**, *322*, 1668–1671. (g) Arduini, A.; Bussolati, R.; Credi, A.; Faimani, G.; Garaudée, S.; Pochini, A.; Secchi, A.; Semeraro, M.; Silvi, S.; Venturi, M. *Chem.-Eur. J.* **2009**, *15*, 3230–3242.

(18) (a) Hori, A.; Yamashita, K.; Fujita, M. *Angew. Chem.* **2004**, *116*, 5126–5129; *Angew. Chem., Int. Ed.* **2004**, *43*, 5016−5019. (b) Yang, C.; Ko, Y. H.; Selvapalam, N.; Origane, Y.; Mori, T.; Wada, T.; Kim, K.; Inoue, Y. *Org. Lett.* **2007**, *9*, 4789–4792. (c) Masson, E.; Lu, X.-Y.; Ling, X.-X.; Patchell, D.-L. *Org. Lett.* **2009**, *11*, 3798–3801. (d) Cangelosi, V. M.; Carter, T. G.; Zakharov, L. N.; Johnson, D. W. *Chem. Commun.* **2009**, 5606–5608. (e) Fujita, M.; Nagao, S.; Ogura, K. *J. Am. Chem. Soc.* **1995**, *117*, 1649–1650. (f) Mukhopadhyay, P.; Zavalij, P. Y.; Isaacs, L. *J. Am. Chem. Soc.* **2006**, *128*, 14093–14102.

Scheme 1. Top, Chemical Structures of Wheel and Axle Components From Which the Pseudorotaxanes Presented Here Are Assembled; Bottom, The Self-Assembling/Self-Sorting Pseudorotaxanes under Study[a]

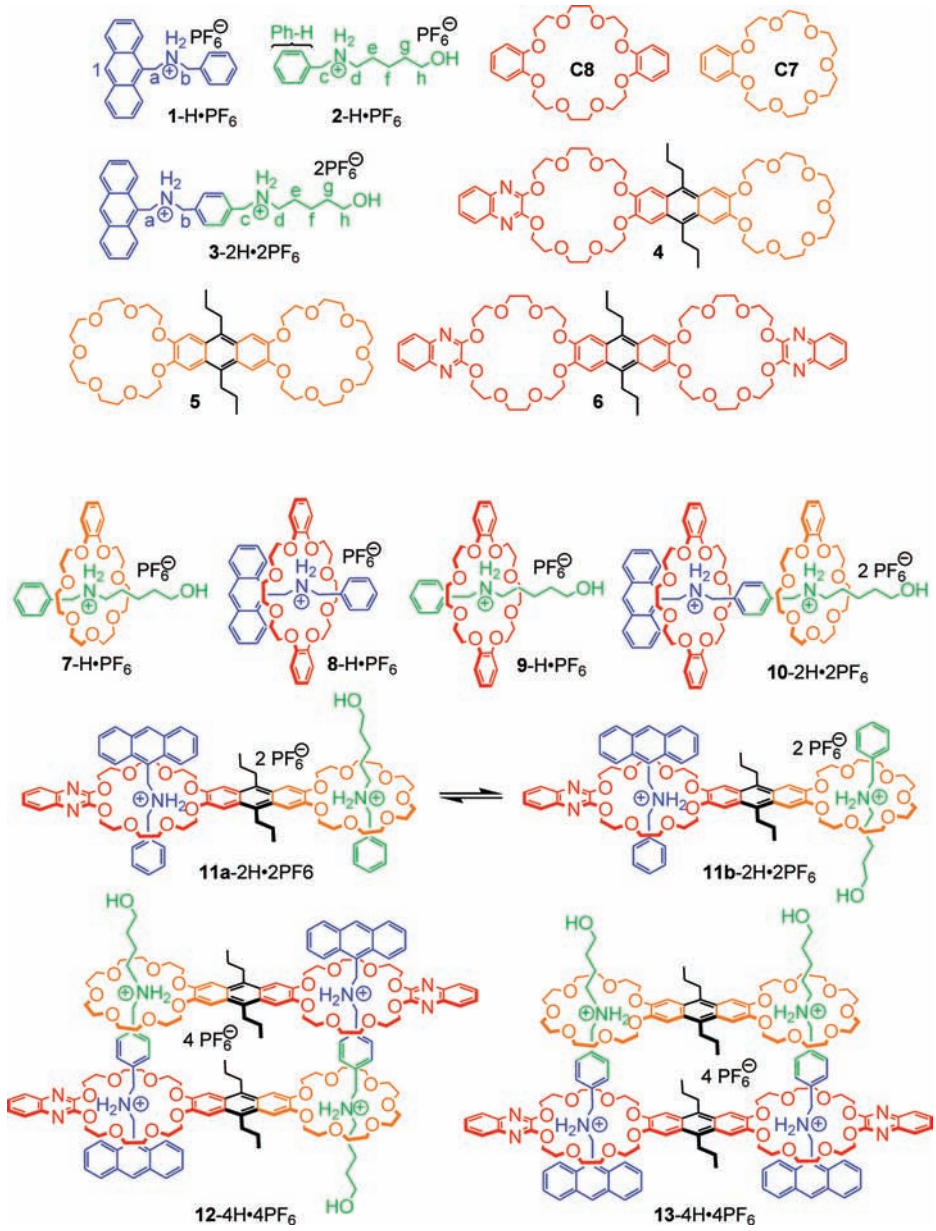

[a] The labeling of axle hydrogen atoms is used in the NMR discussion that follows as shown here.

be extended down to even a second or less. Such a microreactor technique has been applied to the identification of reaction intermediates aiming at understanding the mechanistic details of organic reactions[20] and to the formation processes during the nucleation of inorganic clusters.[14]

In this contribution, ESI-MS and the mixed-flow microreactor are for the first time applied to the investigation of self-sorting pseudorotaxanes. Scheme 1 shows their structures and the corresponding individual components, which have been characterized previously.[12] Assembly intermediates as well as

(19) (a) Claessens, C. G.; Vicente-Arana, M. J.; Torres, T. *Chem. Commun.* **2008**, 6378–6380. (b) Abrecht, M.; Mirtschin, S.; de Groot, M.; Janser, I.; Runsink, J.; Raabe, G.; Kogej, M.; Schalley, C. A.; Fröhlich, R. *J. Am. Chem. Soc.* **2005**, *127*, 10371–10387. (c) Zheng, Y.-R.; Stang, P. J. *J. Am. Chem. Soc.* **2009**, *131*, 3487–3489. (d) Zheng, Y.-R.; Yang, H.-B.; Ghosh, K.; Zhao, L.; Stang, P. J. *Chem.-Eur. J.* **2009**, *15*, 7203–7214. (e) Hasenknopf, B.; Lehn, J.-M.; Boumediene, N.; Leize, E.; Van Dorsselaer, A. *Angew. Chem.* **1998**, *110*, 3458–3460; *Angew. Chem., Int. Ed.* **1998**, *37*, 3265−3268. (f) Albrecht, M.; Dehn, S.; Fröhlich, R. *Angew. Chem.* **2006**, *118*, 2858–2860; *Angew. Chem., Int. Ed.* **2006**, *45*, 2792−2794. (g) Mathieson, J. S.; Cooper, G. J. T.; Pickering, A. L.; Keller, M.; Long, D.-L.; Newton, G. N.; Cronin, L. *Chem. Asian J.* **2009**, *4*, 681–687. (h) Sato, S.; Ishido, Y.; Fujita, M. *J. Am. Chem. Soc.* **2009**, *131*, 6064–6065.

(20) For reviews on studying reaction mechanisms by ESI-MS: (a) Santos, L. S.; Knaack, L.; Metzger, J. O. *Int. J. Mass Spectrom.* **2005**, *246*, 84–104. (b) Eberlin, M. N. *Eur. J. Mass Spectrom.* **2007**, *13*, 19–28. (c) Santos, L. S. *Eur. J. Org. Chem.* **2008**, *23*, 5–253. For recent examples: (d) Santos, L. S.; Metzger, J. O. *Angew. Chem.* **2006**, *118*, 991–99; *Angew. Chem., Int. Ed.* **2006**, *45*, 977−981. (e) Marquez, C. A.; Fabbretti, F.; Metzger, J. O. *Angew. Chem.* **2007**, *119*, 7040–7042; *Angew. Chem., Int. Ed.* **2007**, *46*, 6915−6917. (f) Santos, L. S.; Metzger, J. O. *Rapid Commun. Mass Spectrom.* **2008**, *22*, 898–904. (g) Wang, H.-Y.; Metzger, J. O. *Organometallics* **2008**, *27*, 2761–2766. (h) Marquez, C. A.; Wang, H.-Y.; Fabbretti, F.; Metzger, J. O. *J. Am. Chem. Soc.* **2008**, *130*, 17208–17209. (i) Wang, H.-Y.; Yim, W.-L.; Klüner, T.; Metzger, J. O. *Chem.-Eur. J.* **2009**, *15*, 10948–10959.

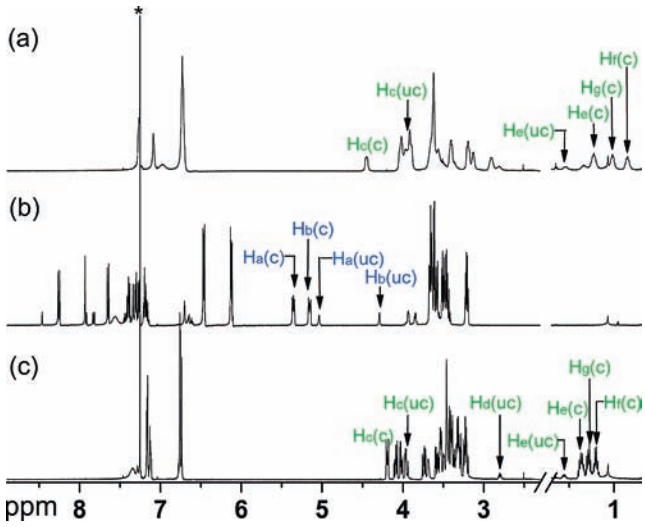

Figure 1. ^{1}H NMR spectra (500 MHz, 298 K, $CDCl_3$:CD_3CN = 2:1, 10.0 mM) of equimolar mixtures of (a) **2**-H·PF_6 and **C8**; (b) **1**-H·PF_6 and **C8**; and (c) **2**-H·PF_6 and **C7** (shown from top to bottom in the order of decreasing exchange rates). Complexed and uncomplexed species are denoted by "c" and "uc" in the parentheses, respectively. Asterisk = solvent.

wrongly assembled structures carrying positive charges could be unambiguously detected by ESI-MS. The information obtained from a simple four-component self-sorting system provides the basis for understanding the formation kinetics of more complex assemblies.

Results and Discussion

Simple Pseudorotaxanes from Combinations of 1-H·PF_6, 2-H·PF_6, C7, and C8. Four binary combinations of the two axles **1**-H·PF_6 and **2**-H·PF_6 and the two crown ethers **C7** and **C8** are in principle possible. One of these, that is, the combination of **1**-H·PF_6 and **C7**, is known not to form a pseudorotaxane,[21] because the axle phenyl group is too large to slip through the smaller crown. Consequently, binding constants and the thermodynamic stability can only be determined for the other three combinations. From earlier literature studies, binding constants in acetone are already available. At 298 K, they are 615 ± 36 M^{-1} (ΔG = −15.9 kJ/mol) for **7**-H·PF_6,[21] 496 ± 18 M^{-1} (ΔG = −15.4 kJ/mol) for **8**-H·PF_6,[12a] and 155 ± 8 M^{-1} (ΔG = −12.5 kJ/mol) for **9**-H·PF_6.[21] We also determined the binding constants at 298 K in significantly less polar $CDCl_3$:CD_3CN = 2:1, which we used for the NMR experiments reported below. They are 14 500 ± 1100 M^{-1} (ΔG = −23.7 kJ/mol) for **7**-H·PF_6, 5500 ± 300 M^{-1} (ΔG = −21.3 kJ/mol) for **8**-H·PF_6, and 1030 ± 30 M^{-1} (ΔG = −17.2 kJ/mol) for **9**-H·PF_6. Thus, the absolute binding constant values increase as expected with lower solvent polarity, but the thermodynamic ranking of the three pseudorotaxanes is **7**-H·PF_6 > **8**-H·PF_6 ≫ **9**-H·PF_6 in both solvents.

Figure 1 shows the NMR spectra of equimolar mixtures of **2**-H·PF_6 and **C8** (Figure 1a), **1**-H·PF_6 and **C8** (Figure 1b), and **2**-H·PF_6 and **C7** (Figure 1c) in a 2:1 mixture of chloroform and acetonitrile. These NMR samples thus contain the pseudorotaxanes **9**-H·PF_6, **8**-H·PF_6, and **7**-H·PF_6, respectively. From a comparison with the spectra of uncomplexed components, a straightforward assignment of signals for the complexed and uncomplexed axles can be achieved. A comparison of the three spectra shows the signals for the complexed and the uncomplexed axle in Figure 1a to appear separately, but to be significantly broadened. This suggests the axle exchange at room temperature to be still slow on the ^{1}H NMR time scale at 500 MHz, but to already approach the point at which peak coalescence would be observed. This observation is in agreement with a report by Busch et al.[22] that similar axles containing alkyl chains shorter than five methylene groups undergo fast exchange in benzo-24-crown-8, while those having more than five methylene groups exchange only slowly (at 298 K, 400 MHz and in acetone-d_6). In contrast, the NMR spectra in Figure 1b,c showed sharp signals, indicating that the axle exchange rates in **7**-H·PF_6 and **8**-H·PF_6 are significantly lower than those for **9**-H·PF_6.

Because these axle exchange reactions will unavoidably occur, when error-correction is to be achieved in a related self-sorting system, it is important to examine the pseudorotaxanes' axle exchange behavior in more detail. ^{1}H,^{1}H EXSY NMR experiments have been performed for the three axle/crown pairs. In each experiment, a 2:1 ratio of axle and crown was used to provide an approximate 1:1 signal ratio for the free and complexed axles. The axle exchange rate constant for **9**-H·PF_6 was determined to be 12 s^{-1} at 14 °C corresponding to a half-life of ca. 85 ms. More than 90% of the axles are thus exchanged within 300 ms. In marked contrast, only a very minor amount of axle exchange was observed for **8**-H·PF_6 after a 600 ms delay and no exchange at all for **7**-H·PF_6 under the same conditions. Therefore, the latter two solutions were heated to 50 °C to make the axle exchange reactions more easily detectable by EXSY NMR experiments. After an 800 ms delay, ca. 10% exchange was observed for **8**-H·PF_6 (corresponding to a half-life at 50 °C of ca. 5.2 s),[23] and again no exchange occurred for **7**-H·PF_6. These results clearly show the order of exchange rates of the three pseudorotaxanes to be **9**-H·PF_6 > **8**-H·PF_6 ≫ **7**-H·PF_6.

Two aspects make self-sorting systems interesting that are based on the above binding motifs: (i) The exchange rates of the three pseudorotaxanes are distinctly different. Consequently, error-correction steps involving different binding motifs can be expected to occur on sufficiently different time scales to provide a rich and interesting kinetic behavior worth studying. (ii) In the case of the present pseudorotaxanes, the kinetic ranking differs from the thermodynamic stability order. The most stable pseudorotaxane **7**-H·PF_6 forms at the lowest rate, and the least stable complex **9**-H·PF_6 is the fastest one to appear. In this situation, errors are to be expected to occur during the self-assembly/self-sorting process. Consequently, it should be possible to detect significant amounts of wrongly assembled complexes and to follow the subsequent error-correction steps, if the experimental methods operate on suitable time scales.

ESI-FTICR Mass Spectrometry as a Tool To Study Self-Sorting Processes. The two binding motifs on which the assemblies in Scheme 1 are based are quite similar. In a mixture

(21) Zhang, C.-J.; Li, S.-J.; Zhang, J.-Q.; Zhu, K.-L.; Li, N.; Huang, F.-H. *Org. Lett.* **2007**, *9*, 5553–5556.

(22) Clifford, T.; Abushamleh, A.; Busch, D. H. *Proc. Natl. Acad. Sci. U.S.A.* **2002**, *99*, 4830–4836.

(23) It should be briefly noted that chloroform:acetonitrile 2:1 was used for the NMR experiments because of solubility reasons. For the mass spectrometric experiments, which are performed at a significantly lower building block concentration, dichloromethane:acetonitrile 8:1 could be used. By using a more unpolar solvent, the self-sorting fidelity can be increased, and a more clear-cut picture evolves from the experiment. Consequently, the time scales might be somewhat different, but our results clearly show that the relative order of rate constants remains the same.

containing the free building blocks, wrongly assembled complexes, assembly intermediates, and the thermodynamic product complexes, NMR experiments become difficult to interpret because of a severe superposition of signals (one example is shown in the Supporting Information, Figure S1). Therefore, we decided to use electrospray Fourier-transform ion-cyclotron-resonance (ESI-FTICR) mass spectrometry. Because of the high resolution, signal assignment is straightforward from the isotope patterns and the exact masses, even in cases where different species overlap. The high sensitivity of modern mass spectrometers also permits the detection of some low-concentration intermediates.

Three potential sources for errors or misinterpretations of mass spectrometric experiments should be briefly discussed: (i) Ionization artifacts may occur. ESI MS often produces so-called unspecific aggregates. In the case of the pseudorotaxanes under study, such an unspecific aggregate might be a nonthreaded, side-on complex of a crown ether and an axle that just forms during ionization, but is absent in solution. However, we recently[12,24] used ESI-MS to characterize the pseudorotaxanes through their gas-phase fragmentation reactions. No significant contributions originating from unspecific aggregation have been observed. Neither contain the spectra presented here any indication of larger amounts of such aggregates (see below). (ii) Noncovalent complexes may dissociate during ionization, even when a soft ionization method such as ESI is used. The ionization conditions of all experiments discussed here have been optimized to minimize or even completely avoid such fragmentation reactions in the ion source. This was tested with the final equilibrium mixtures of the pseudorotaxanes in Scheme 1, which only showed signals for the expected assemblies, thus ruling out prominent fragmentation reactions during ionization (see below). (iii) The peak intensities in mass spectra do not necessarily reflect the solution concentrations.[25] In the spectra discussed below, only very minor signals are seen for uncomplexed crown ethers, because they are neutral, and low concentration background ions such as H^+, NH_4^+, Na^+, and K^+ are needed to generate detectable ions. Also, the free axles are hardly visible, because they form quite strong ion pairs[26] in the rather unpolar spray solvent chosen (CH_2Cl_2:CH_3CN = 8:1).[23] The pseudorotaxanes, however, are easy to ionize by stripping off a counterion, which has already been halfway displaced from the vicinity of the positive charge by the complexed crown ether. Consequently, we only discuss changes in the intensities of pseudorotaxane ions. Changes in their relative intensities over time provide at least semiquantitative information on the changes occurring in solution.

A second point is how MS experiments can be performed on shorter time scales. In this study, slow processes occurring on a time scale longer than 2 min were monitored by simply taking mass spectra at different reaction times after mixing the corresponding building blocks in a vial. Fast processes on time scales shorter than 2 min were instead monitored by coupling a mixed-flow microreactor[14,20] to the ESI ion source (Figure 2). Two reactant solutions (both CH_2Cl_2:CH_3CN = 8:1, 500 μM reactant concentration) in two separate identical syringes

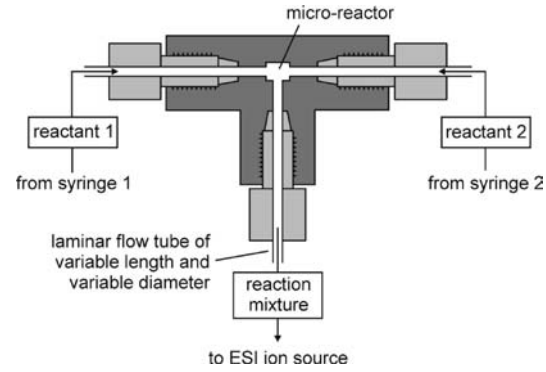

Figure 2. The ESI-MS-coupled mixed-flow microreactor for studying short-time kinetics. Two reactant solutions are mixed in the microreactor. The reactions proceed during the time needed for the transport of the mixed solution to the tip of the ESI capillary.

are pumped with the same flow rate through two identical capillaries into the microreactor where they are thoroughly mixed. The resulting mixture (250 μM in each component) is introduced into the ESI ion source. The length and diameter of the capillary connecting the microreactor with the ESI ion source and the flow rate determine the reaction time. Through varying these parameters, reaction kinetics can be measured down to reaction intervals of about one-half a second.

A Four-Component Self-Sorting System. After mixing the two axles **1**-H·PF_6 and **2**-H·PF_6 (combined in syringe 1 for the microreactor experiments) with the two crown ethers **C7** and **C8** (combined in syringe 2), the two pseudorotaxanes containing **C8**, that is, **8**-H·PF_6 and **9**-H·PF_6, are already detected after a reaction time of 22 s as the two major ions [**8**-H]$^+$ at *m*/*z* 746 and [**9**-H]$^+$ at *m*/*z* 642 (Figure 3a). In line with the EXSY NMR experiments discussed above, these two complexes thus assemble quickly. At longer reaction times, [**7**-H]$^+$ begins to appear at *m*/*z* 550. Even after 40 min reaction time, significant amounts of wrongly assembled **9**-H·PF_6 are visible, which almost completely vanish within 15 h. The mass spectra thus are in agreement with the NMR results and show the quick equilibration of **8**-H·PF_6 and **9**-H·PF_6, which are interdependent because the two axles compete for the same **C8** crown ether. The latter pseudorotaxane is finally consumed in a slow error-correction step to yield the two thermodynamically favored self-sorting products **7**-H·PF_6 and **8**-H·PF_6.

Sequence-Specific Pseudorotaxanes: A Streamlined Formation Pathway. Sequence-specific assemblies are generally interesting because they store information. Pseudorotaxane **10**-2H·$2PF_6$ combines both binding sites in one axle and thus binds both crown ethers in a specific sequence.[12a] Because the anthracene moiety is blocking any threading step, the threading events must proceed in correct order to achieve the thermodynamic product with the correct crown ether sequence. First, axle **3**-2H·$2PF_6$ needs to thread into the cavity of **C8**. In a second step, **C8** needs to move from the hydroxypentyl ammonium station (for simplicity from now on called the "green binding site" according to the colors in the figures) of the axle to the anthracenyl methyl ammonium part (the "blue binding site"). Finally, **C**7 can slip onto the free green binding site. Otherwise, **C7** would block the way of **C8** to reach the blue binding site. The corresponding mass spectra are shown in Figure 4. The formation of **10**-2H·$2PF_6$ commences with the competition of **C7** and **C8** for the green binding site in **3**-2H·$2PF_6$. The barrier for slipping **C7** over the green binding site is, however, much higher than that for **C8**. Consequently, pseudorotaxane **15**-

(24) Jiang, W.; Schalley, C. A. *Anal. Chem.*, submitted for publication.
(25) Leize, E.; Jaffrezic, A.; Van Dorsselaer, A. *J. Mass Spectrom.* **1996**, *31*, 537–544.
(26) (a) Jones, J. W.; Gibson, H. W. *J. Am. Chem. Soc.* **2003**, *125*, 7001–7004. (b) Huang, F.-H.; Jones, J. W.; Slebodnick, C.; Gibson, H. W. *J. Am. Chem. Soc.* **2003**, *125*, 14458–14464. (c) Gasa, T. B.; Spruell, J. M.; Dichtel, W. R.; Sorensen, T. J.; Philp, D.; Stoddart, J. F.; Kuzmic, P. *Chem.-Eur. J.* **2009**, *15*, 106–116.

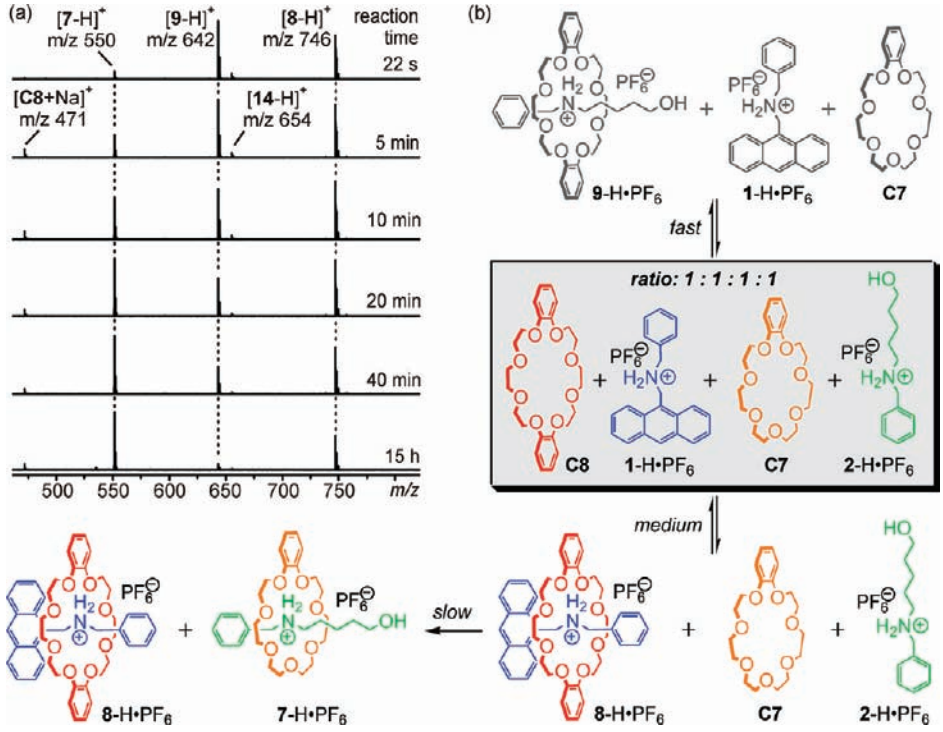

Figure 3. (a) ESI-FTICR mass spectra of an equimolar mixture of **1**-H•PF_6, **2**-H•PF_6 (combined in syringe 1), **C7**, and **C8** (combined in syringe 2) recorded after different reaction times (295 K, CH_2Cl_2:CH_3CN = 8:1, 250 μM). The very minor signal at *m*/*z* 654 for [**14**-H^+] corresponds to an unspecific side-on complex of **1**-H•PF_6 and **C7** and illustrates that they do not play a significant role. (b) Formation pathways of **7**-H•PF_6 and **8**-H•PF_6 as identified from the spectra. The gray box indicates the starting point, here the four free components of the mixture. The gray structures represent a quickly formed assembly error, which is corrected in the process of the reaction.

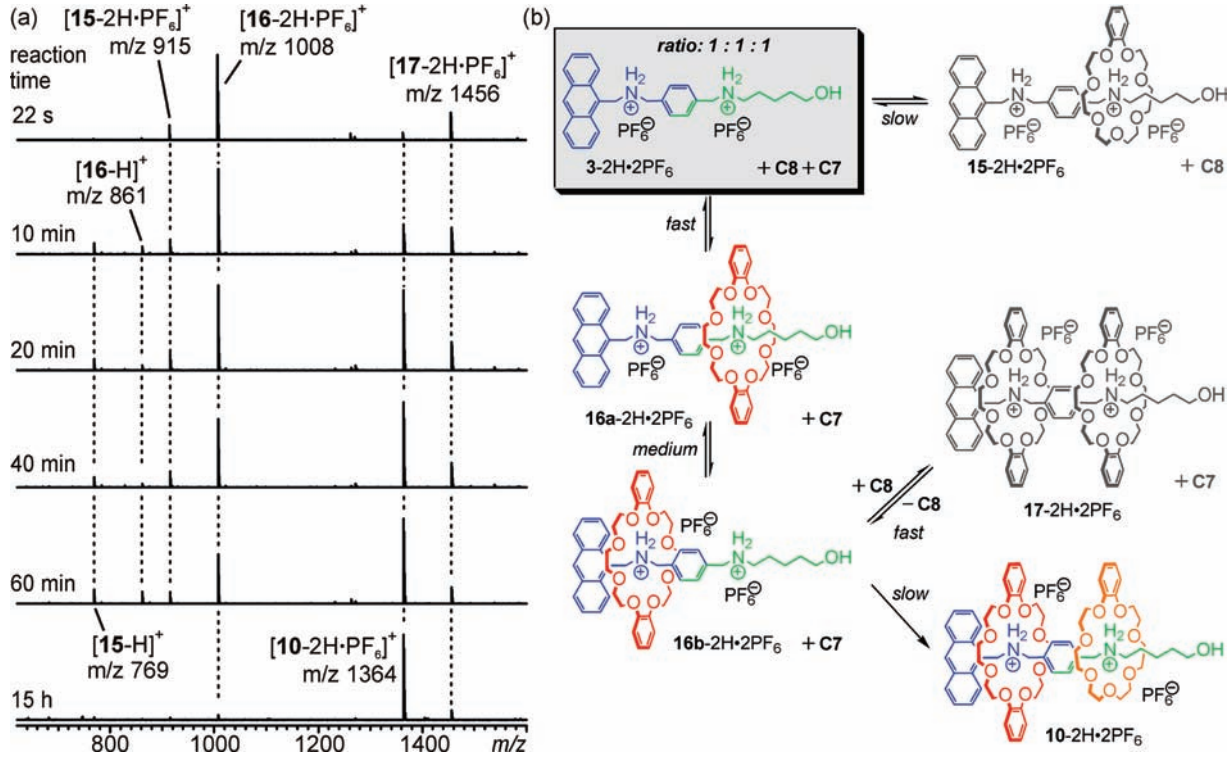

Figure 4. (a) ESI-FTICR mass spectra of an equimolar mixture of **C7**, **C8** (syringe 1), and **3**-2H•$2PF_6$ (syringe 2) recorded after different reaction times (295 K, CH_2Cl_2:CH_3CN = 8:1, 250 μM). (b) Formation pathways of **10**-2H•$2PF_6$ as identified from the MS results. The gray structures represent dead ends that require error-correction. Note that **16a**-2H•$2PF_6$ and **16b**-2H•$2PF_6$ are isobaric and thus cannot be distinguished by their mass-to-charge ratio.

2H•$2PF_6$ is formed only to a minor extent, while most of the green part of the axle is occupied by kinetically preferred **C8** yielding **16a**-2H•$2PF_6$. This is indicated by the major signal for [**16**-2H•PF_6]$^+$ at *m*/*z* 1008 and the very minor signal for [**15**-2H•PF_6]$^+$ at *m*/*z* 915. In the second, somewhat slower **C8** migration to the blue part of the axle, **16b**-2H•$2PF_6$ is generated.

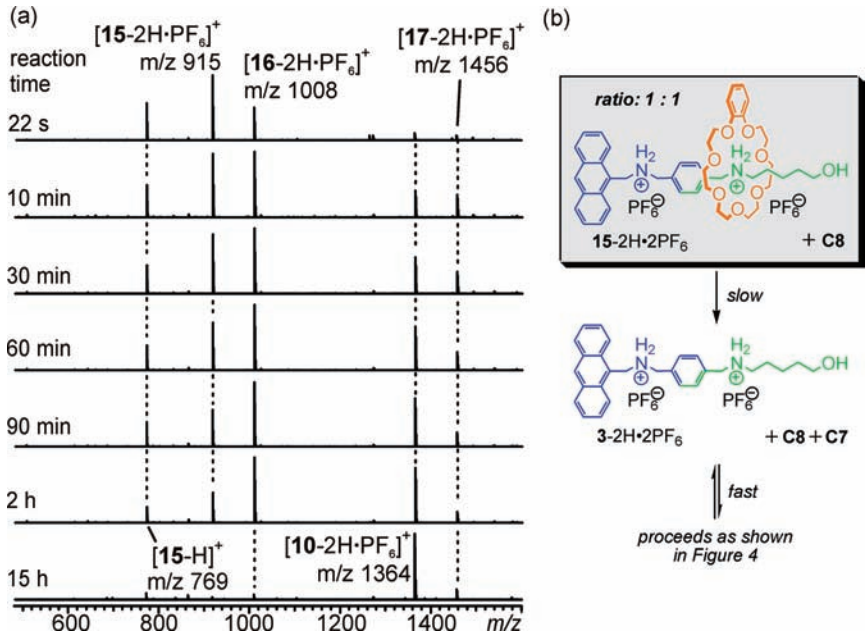

Figure 5. (a) ESI-FTICR mass spectra of an equimolar mixture of **C8** (syringe 1) and preformed **15**-2H·2PF$_6$ (syringe 2) recorded after different reaction times (295 K, CH_2Cl_2:CH_3CN = 8:1, 250 μM). (b) The new starting point is indicated by the gray box. After slow dissociation of **15**-2H·2PF$_6$, the reaction proceeds as shown in Figure 4.

Its presence in the mixture cannot be directly detected, because it is merely a positional isomer of **16a**-2H·2PF$_6$ and thus appears at the same *m*/*z*. However, the observation of [**17**-2H·PF$_6$]$^+$ indicates the **C8** migration to occur already to some extent at the early stages of the experiment. Two **C8** crown ethers can only bind to the axle, when the first **C8** has already reached its final position. The last step in which **16b**-2H·2PF$_6$ is converted to **10**-2H·2PF$_6$ by threading of the green part of the axle through **C7** is again slow.

In the threading sequence, all steps occur with decreasing rates. The first step is the fastest, while the final step is the slowest. This results in an accumulation of the intermediate complexes in each step. Consequently, the concentration of **16a**-2H·2PF$_6$ is high, making the subsequent reaction efficient. Again, **16b**-2H·2PF$_6$ accumulates before the last slow step occurs, and its higher concentration will make the last step efficient. In this sense, the ranking of threading rates is streamlined to favor the productive pathway, while dead-end structures either form only in minor amounts (such as **15**-2H·2PF$_6$) or are in fast equilibria with the assembly intermediates (like **17**-2H·2PF$_6$) and thus do not hamper the subsequent assembly step much.

As a control experiment, **15**-2H·2PF$_6$ was preformed by mixing **3**-2H·2PF$_6$ and **C7** in a 1:1 ratio (for a characterization of **15**-2H·2PF$_6$ by NMR and MS experiments, see Figures S2 and S3 in the Supporting Information). After equilibration of this mixture for one day, **C8** was added in an equimolar ratio, and the conversion to **10**-2H·2PF$_6$ was monitored over time. Only when **15**-2H·2PF$_6$ dissociates back into its components is the error corrected. This step, however, is slow. In the mass spectra (Figure 5), intense signals for **15**-2H·2PF$_6$ appear: [**15**-H]$^+$ at *m*/*z* 769 and [**15**-2H·PF$_6$]$^+$ at *m*/*z* 915. The free axle formed during the slow dissociation of **15**-2H·2PF$_6$ finds a high concentration of **C8** competing with a low concentration of **C7**. Consequently, [**16**-2H·PF$_6$]$^+$ and [**17**-2H·PF$_6$]$^+$ form in significant amounts. The final step, threading of **C7** onto the green part of **16b**-2H·2PF$_6$, is again slow.

If one compares, for example, the spectra in Figures 4 and 5 that were obtained after a reaction time of 60 min, it becomes obvious that the error-correction is more time-consuming when **15**-2H·2PF$_6$ and **C8** are used as the starting point rather than the free components. While we observe an approximate 1:2 ratio of [**16**-2H·PF$_6$]$^+$ and [**10**-2H·PF$_6$]$^+$ after 60 min in Figure 4, the ratio of these ions is roughly 3:2 in the corresponding spectrum in Figure 5. This difference is due to the repository effect of **15**-2H·2PF$_6$. It liberates free axle and free **C7** only slowly, thus keeping the concentration of these components low for the subsequent assembly steps that finally yield **10**-2H·2PF$_6$.

Pseudorotaxanes from Monotopic Axles and a Crown Ether Heterodimer. In marked contrast to the sequence-specific pseudorotaxanes, the formation of pseudorotaxane **11**-2H·2PF$_6$ from an equimolar mixture of axles **1**-H·PF$_6$ and **2**-H·PF$_6$ and the crown ether heterodimer **4** does not require the threading events to occur consecutively in a well-defined sequence. Figure 6 shows the results obtained for this system.

At very short reaction times of 0.6 s after mixing, **1**-H·PF$_6$ and **2**-H·PF$_6$ with **4**, only ions for pseudorotaxanes bearing just one of the two axles appear: [**18**-H]$^+$ is observed at *m*/*z* 1156 and [**19**-H]$^+$ at *m*/*z* 1260. Because the threading of **2**-H·PF$_6$ into the 21-crown-7 part of the crown heterodimer is certainly slow, it is unlikely that **18b**-H·PF$_6$ is formed with high concentration. Consequently, the by far major fraction of the ions appearing at *m*/*z* 1156 corresponds to [**18a**-H]$^+$ in which **2**-H·PF$_6$ is threaded into the 24-crown-8 part of **4**. Between 0.6 and 22 s reaction time, the relative intensities of [**18**-H]$^+$ and [**19**-H]$^+$ undergo an obvious change from an approximate 2:3 to a 3:2 ratio. This change is due to the fact that the thinner axle **2**-H·PF$_6$ slips into the 24-crown-8 within some tenths of a second, while the threading of **1**-H·PF$_6$ occurs within several seconds. The competition between **1**-H·PF$_6$ and **2**-H·PF$_6$ for the 24-crown-8 unit of **4** thus reaches equilibrium only within about the first minute or so. This is also supported by the fact that the intensity ratio of [**18**-H]$^+$ and [**19**-H]$^+$ remains almost constant for the next couple of minutes (cf., the spectrum

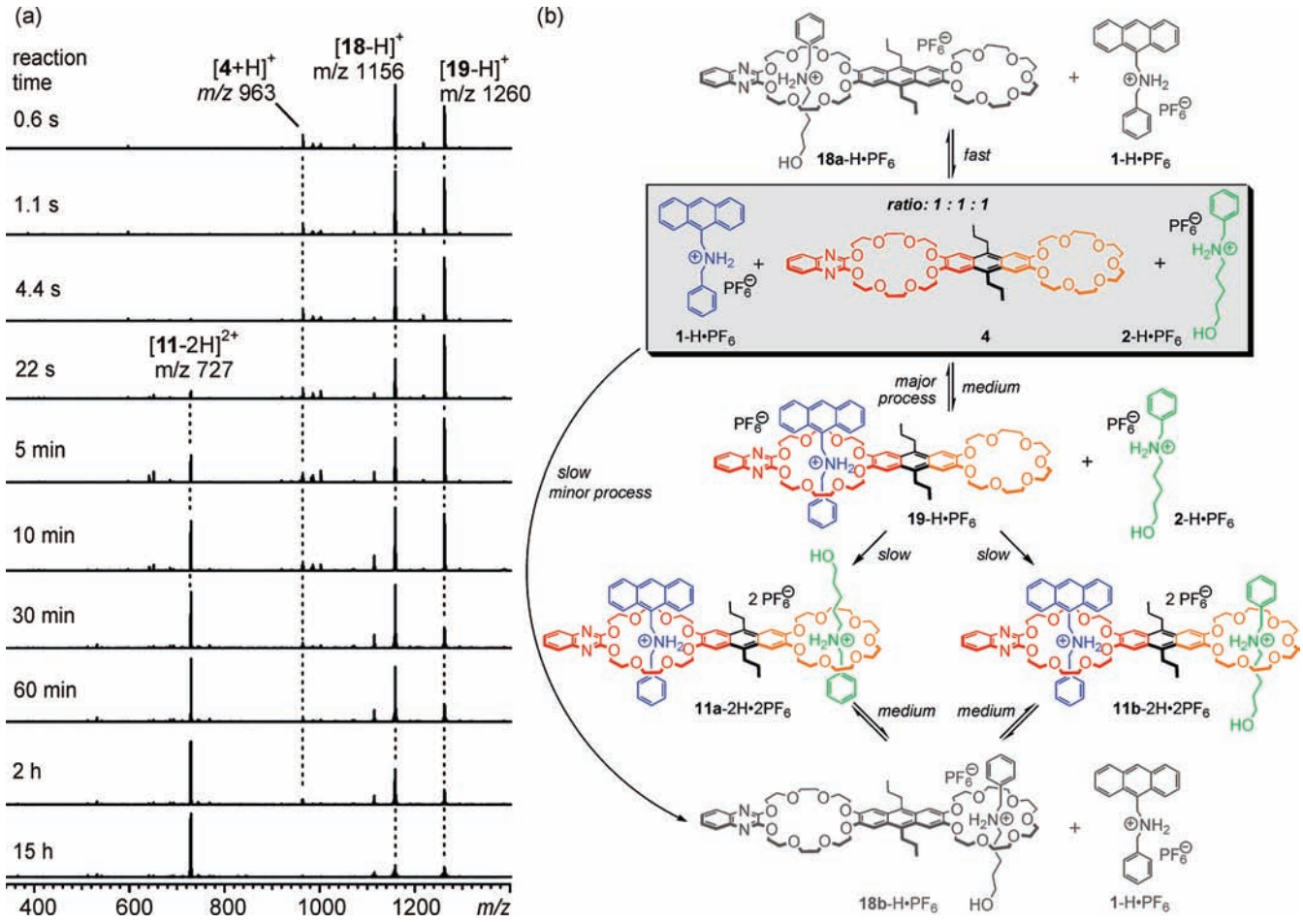

Figure 6. (a) ESI-FTICR mass spectra of an equimolar mixture of **1**-H·PF_6 and **2**-H·PF_6 (syringe 1) with **4** (syringe 2) recorded after different reaction times (295K, CH_2Cl_2:CH_3CN = 8:1, 250 μM). (b) Formation pathways of **11**-2H·2PF_6. The main productive pathways are shown in colors, while wrongly assembled or minor structures appear in gray.

obtained after 5 min). After longer reaction times, the final assembly product [**11**-2H]$^{2+}$ starts to appear at *m*/*z* 727. Both ions [**18**-H]$^+$ and [**19**-H]$^+$ vanish accordingly (also see the NMR experiments depicted in Figure S1, Supporting Information).

Three control experiments confirm this interpretation. In the first experiment (Figure 7a), **18b**-H·PF_6 is preformed by letting axle **2**-H·PF_6 and the crown dimer **4** equilibrate for a day. Because the binding constant of **2**-H·PF_6 binding to **C7** is higher than that for binding of this axle in **C8**, **18b**-H·PF_6 is the major complex in solution (for MS and NMR data confirming this, see Figures S4 and S5, Supporting Information). When the second axle, **1**-H·PF_6, is added to this mixture, it quickly slips into the 24-crown-8 part of **4** and generates the final product **11**-2H·2PF_6. Already after 22 s, more than 75% of the conversion has taken place. When preformed **18b**-H·PF_6 is mixed with both axles in a 1:1:1 ratio (Figure 7b), the 21-crown-7 part of **4** is occupied, and the two axles compete for the free 24-crown-8 binding site. At short reaction times (1.1 s), two [3]pseudorotaxanes are observed: the final product **11**-2H·2PF_6 and, with almost twice its intensity, **20**-2H·2PF_6, the crown dimer **4**, which carries two identical axles **2**-H·PF_6 (also see Figures S4 and S5). After 22 s, **11**-2H·2PF_6 is already the most prominent pseudorotaxane, and the wrongly assembled structure **20**-2H·2PF_6 represents only a minor species (also see Figures S4 and S9). In both of these experiments, **19**-H·PF_6 is not formed to a significant extent, because this would involve a slow dethreading step in which axle **2**-H·PF_6 dissociates from any of the other pseudorotaxanes. In the last of the three control experiments (Figure 7c), **19**-H·PF_6 was preformed (also see Figures S4 and S8) and then mixed with axle **2**-H·PF_6 in equimolar amounts. From the assembly mechanism in Figure 6b, one would expect that the threading of axle **2**-H·PF_6 into the 21-crown-7 part of the crown dimer is so slow that **19**-H·PF_6 dissociates in part and both axles compete for the 24-crown-8 part of **4**. Consequently, the two [2]pseudorotaxanes ions [**18**-H]$^+$ and [**19**-H]$^+$ are both expected to appear quite quickly in the mass spectra. Afterward, the corresponding assemblies should be slowly consumed in the formation of **11**-2H·2PF_6. This is exactly observed in the mass spectra shown in Figure 7c.

Multiply Threaded Pseudorotaxanes. The last two assemblies to be discussed here bear four threading sites and are thus even more complex. In **12**-4H·4PF_6, the ditopic axle **3**-2H·2PF_6 is combined with the crown ether heterodimer **4** in a 1:1 ratio. A 2:2 complex finally assembles in which the two axles as well as the two crown ether dimers are antiparallel to each other. In **13**-4H·4PF_6, 2 equiv of the same axle is combined with 1 equiv of each of the two crown ether homodimers **5** and **6**. In this pseudorotaxane architecture, the two axles are parallel to each other, and the two crown ether dimers appear again in a specific sequence. The self-assembly/self-sorting programmed into the building blocks thus provides full positional control over the subunits in the pseudorotaxane assemblies.[12b] In both of these assemblies, the number of potential formation pathways is again

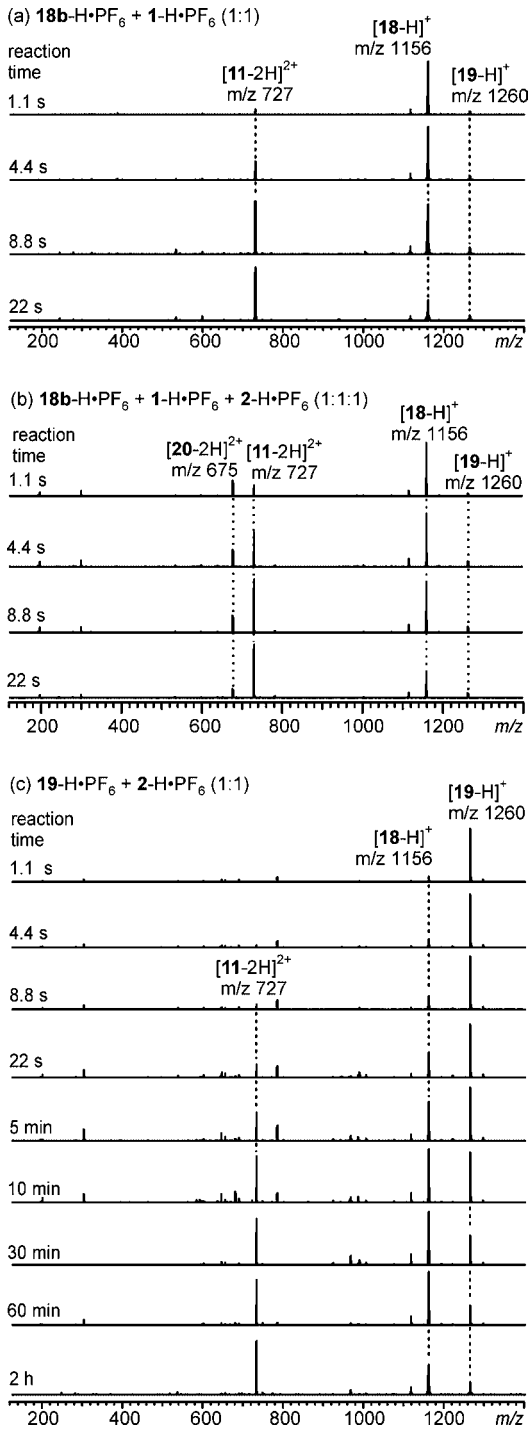

Figure 7. Three control experiments using different starting points for the assembly of **11**-2H·2PF$_6$: (a) equimolar mixture of **18b**-H·PF$_6$ and **1**-H·PF$_6$, (b) equimolar mixture of **18b**-H·PF$_6$ (syringe 1) and **1**-H·PF$_6$ and **2**-H·PF$_6$ (syringe 2), and (c) equimolar mixture of **19**-H·PF$_6$ and **2**-H·PF$_6$.

reduced through the axle, which allows the threading steps only to occur from one end.

Figure 8 shows the mass spectra obtained after different reaction times during the formation of **12**-4H·4PF$_6$. Scheme 2 depicts the corresponding assembly pathways. Besides a minor signal for the protonated crown ether heterodimer [**4**+H]$^+$, only two signals are observed after 22 s reaction time: the 1:1 complex of axle and wheel [**21**-2H]$^{2+}$ at *m*/*z* 689 and a low-intensity signal for [**22**-2H]$^{2+}$. At these short reaction times, the latter signal must correspond to **22a**-2H·2PF$_6$, a pseudorotaxane, where two crown ether heterodimers have been slipped onto the axle with their 24-crown-8 unit. Over time, the final assembly product appears in two charge states, that is, [**12**-4H·PF$_6$]$^{3+}$ at *m*/*z* 967 and [**12**-4H]$^{4+}$ at *m*/*z* 689. The quadruply charged ion has twice the mass and bears twice the number of charges as the 1:1 complex [**21**-2H]$^+$. It correspondingly appears at the same *m*/*z*. Because of the smaller peak spacing in the isotope pattern of 0.25 mass units, the 2:2 pseudorotaxane can easily be distinguished from its 1:1 precursor.

In agreement with the order of threading rates, **21a**-2H·2PF$_6$ is quickly formed from the two free building blocks. Somewhat more slowly, it is transformed into **21b**-2H·2PF$_6$ by migration of the crown ether to the blue binding site of the axle. At this stage, all further reactions that might occur are slow steps with one exception: A second crown dimer **4** can slip over the green part of the axle in **21b**-2H·2PF$_6$ to yield **22a**-2H·2PF$_6$. This process is not prominent, because the crown ether dimer and the axle are present in a 1:1 ratio and most of **4** is thus already consumed by the axle, leaving only a very low concentration of free crown dimer for the formation of **22a**-2H·2PF$_6$. Because **21b**-2H·2PF$_6$ now accumulates, the most prominent reaction on the way to **12**-4H·4PF$_6$ is a dimerization of **21b**-2H·2PF$_6$, which requires two slow steps in which the 21-crown-7 part of **4** slips over the unoccupied green axle binding sites.

Again, we deal with a streamlined formation process here as observed for the sequence-specific pseudorotaxane **9**-2H·2PF$_6$ above. The consequence is that one particularly prominent formation pathway exists leading to clean and simple mass spectra, which are easy to interpret. All of the species observed in the mass spectra and their intensity changes are in good agreement with the kinetic ranking of the threading steps.

This is quite different from the situation encountered during the formation of **13**-4H·4PF$_6$ (Figure 9 and Scheme 3). Although again one intermediate, that is, **24**-2H·2PF$_6$ appearing as [**24**-2H]$^{2+}$ at *m*/*z* 761, is prominent at the beginning, several other intermediates are seen in the spectra. Because 2 equiv of the axle is present in the solution relative to the crown ether dimer **6**, 2:1 complexes **25**-4H·4PF$_6$ are formed and become visible in the mass spectra in different charge states.[27] In Scheme 3, a dotted line indicates that any reaction toward the end product will be slow. Consequently, **24**-2H·2PF$_6$ is in equilibrium with **25a**-4H·4PF$_6$, **25b**-4H·4PF$_6$, and the free components. This explains why the mass spectra are more complex than those obtained during the formation of **12**-4H·4PF$_6$. Also, **26**-2H·2PF$_6$ and **28**-2H·2PF$_6$ are observed with low abundance. Open-chain complexes **27**-4H·4PF$_6$ are certainly present before the final assembly is generated, but cannot be distinguished easily by mass spectrometry, because they are isobaric with the final assembly product. Complexes **26**-2H·2PF$_6$ and **27**-4H·4PF$_6$ can be expected to form with low concentration, because their

(27) It should be noted that NMR results (Figures S10 and S11, Supporting Information) indicate most of the axle to initially be bound to the crown ether homodimer **6**. In the mass spectra, however, the ions corresponding to these complexes, that is, **25a**-4H·4PF$_6$ and **25b**-4H·4PF$_6$, appear only with quite low intensity, while signals corresponding to **24**-4H·4PF$_6$ are significantly more prominent. A potential explanation for this discrepancy might be that charge repulsion increases much upon transition from solution to the gas phase. Consequently, ions generated from **25**-4H·4PF$_6$ may easily dissociate in the gas phase and yield [**24**-2H]$^{2+}$. This is the only case in our study in which such a discrepancy between NMR and MS experiments is observed and in which such a prominent fragmentation reaction appears to proceed.

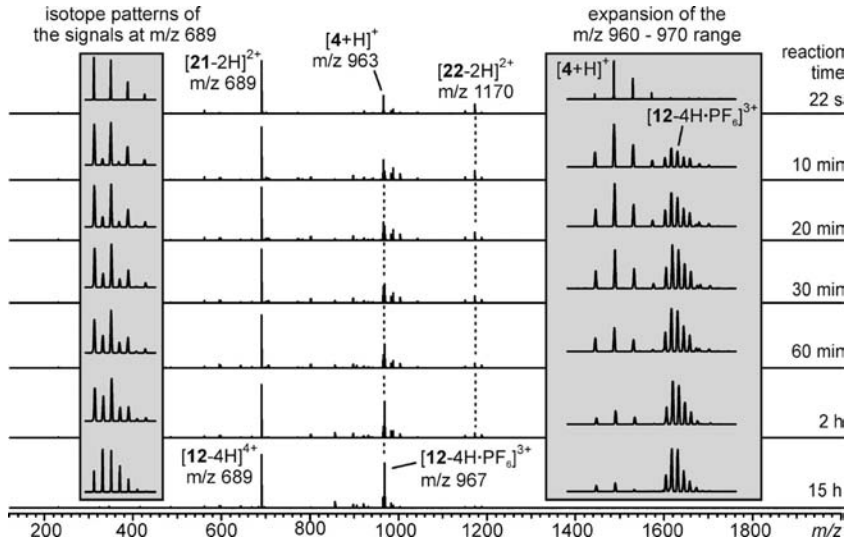

Figure 8. (a) ESI-FTICR mass spectra (295 K, CH_2Cl_2:CH_3CN = 8:1, 250 μM) of an equimolar mixture of **4** with **3**-2H·2PF_6 recorded after different reaction times. The left inset shows the isotope patterns of the signal at *m*/*z* 689. Both [**21**-2H]$^{2+}$ and [**12**-4H]$^{4+}$ appear at the same *m*/*z*, but can clearly be distinguished by the peak spacing in the isotope pattern. The right inset is an expansion of the *m*/*z* = 960−970 area showing that [**4**+H]$^{+}$ and [**12**-4H·PF_6]$^{3+}$ appear right next to each other.

Scheme 2. Assembly Pathways Generating the Antiparallel **12**-4H·4PF_6 Pseudorotaxane Assembly[a]

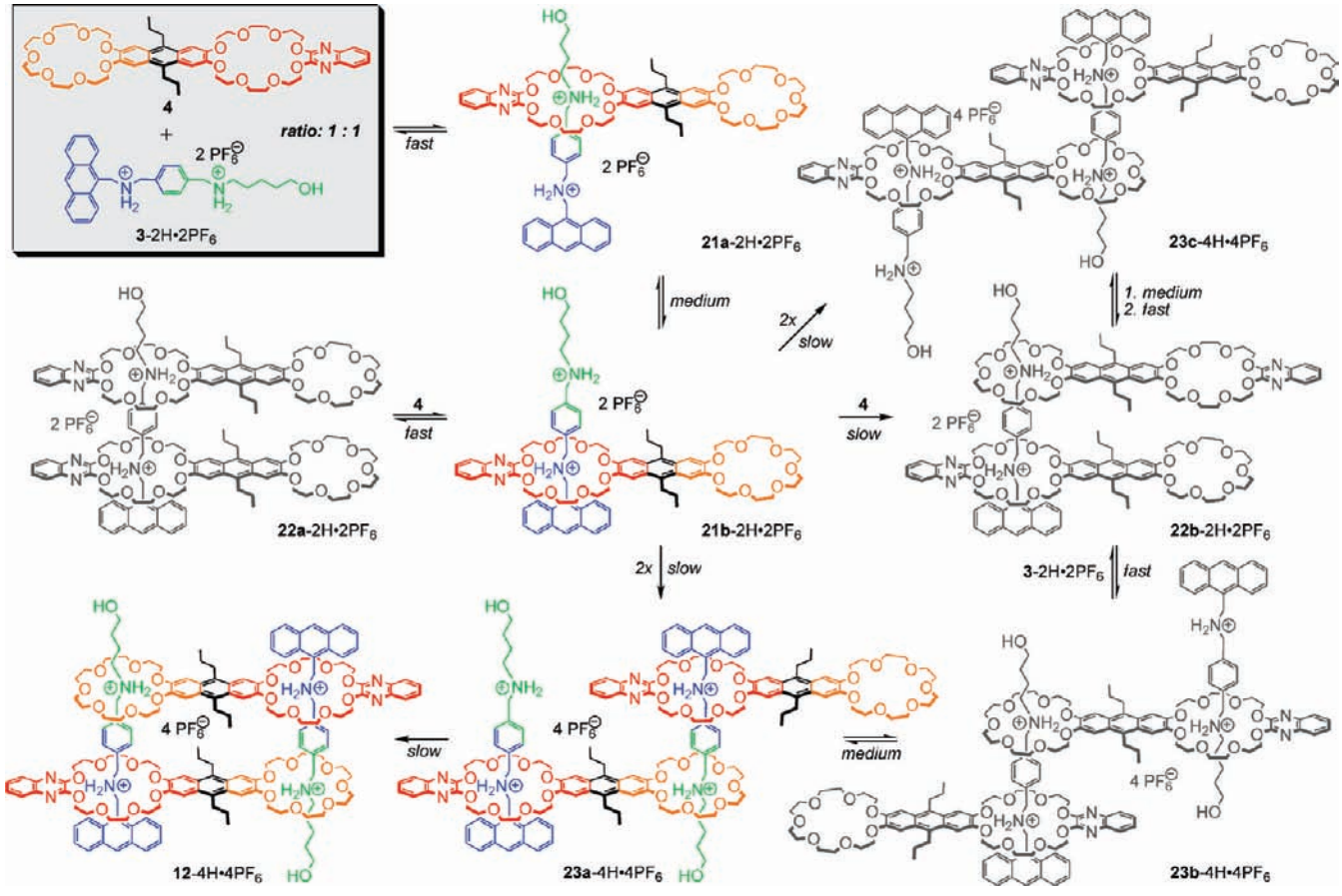

[a] The major productive pathway is shown in colors.

formation is similarly slow as their consumption in the formation of **13**-4H·4PF_6.

Conclusions

The combination of self-assembly with self-sorting allows one to program the assembly of a variety of different pseudorotaxane architectures from a set of simple subunits in a way that finally leads to geometrically well-defined, multiply threaded structures. The pseudorotaxanes under study form on quite distinct time scales depending on the axle−wheel combination. Furthermore, the order of axle exchange rates is significantly different from the thermodynamic stabilities. The most quickly

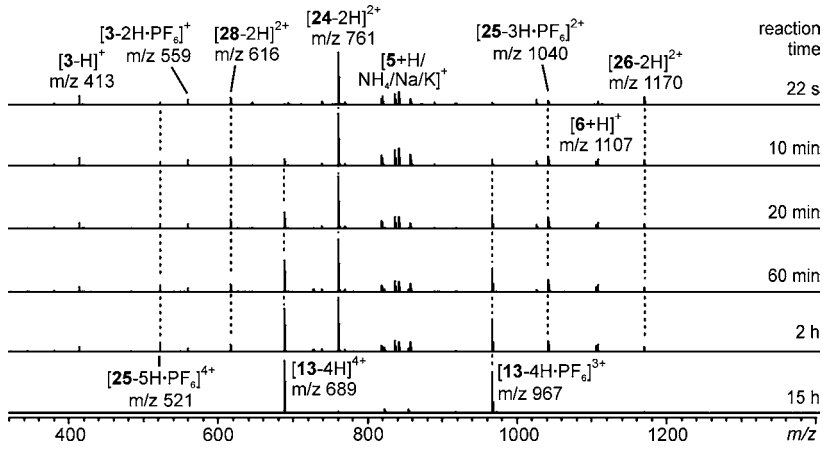

Figure 9. ESI-FTICR mass spectra of a mixture of **5**, **6**, and **3**-2H·2PF$_6$ in 1:1:2 ratio ([**3**-2H·2PF$_6$] = 250 μM; 295 K, CH_2Cl_2:CH_3CN = 8:1) recorded after different reaction times.

Scheme 3. Formation Pathways of **13**-4H·4PF$_6$[a]

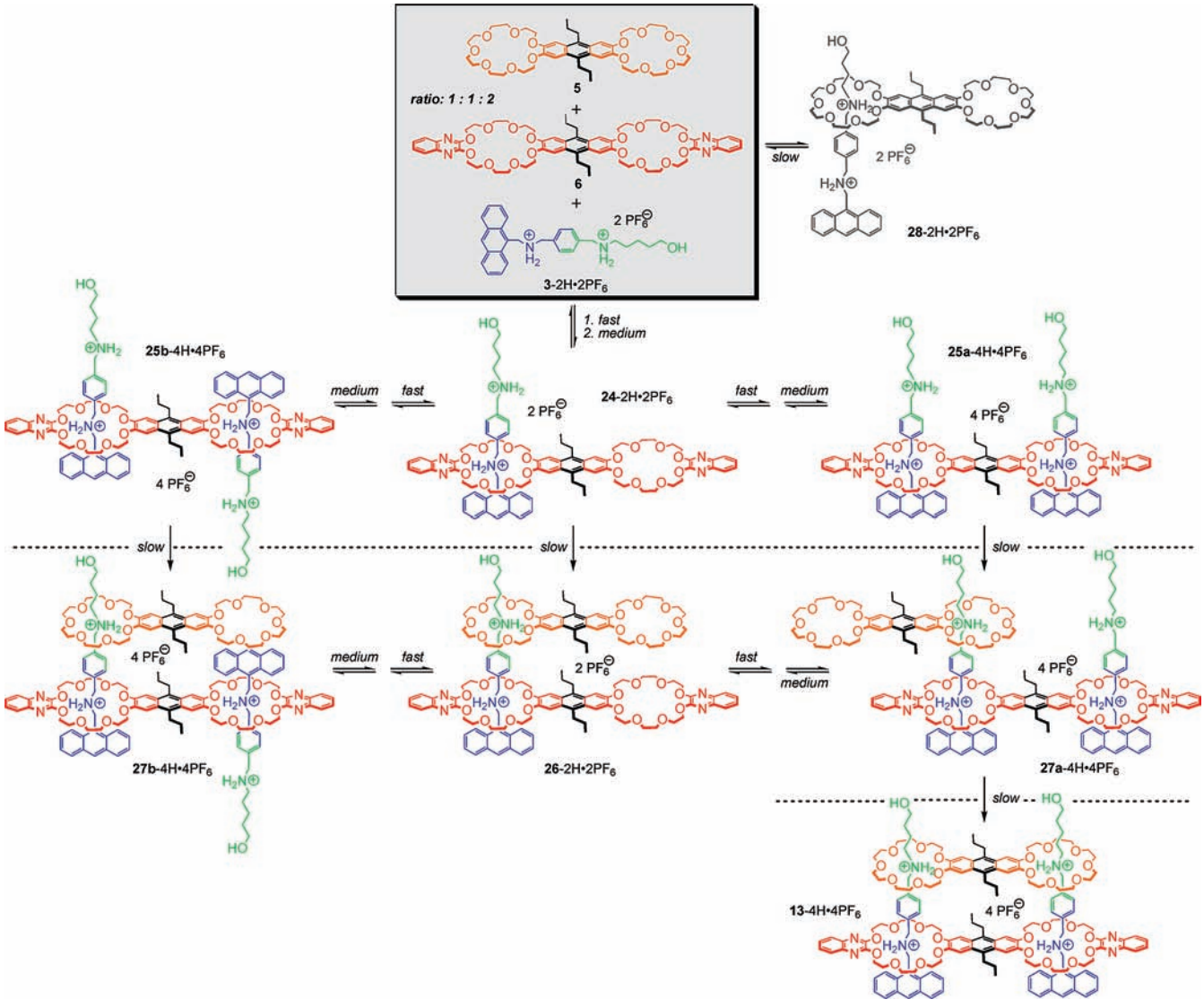

[a] The dotted lines indicate a situation where only the slow step leads closer to the formation of the final self-assembly product. Consequently, all structures above each of the lines are in equilibrium with each other.

exchanging pseudorotaxane **9**-H·PF$_6$ is the least stable, while the most stable pseudorotaxane **7**-H·PF$_6$ exchanges axles within a multiminute time frame. This difference between the order of rates and thermodynamic stabilities unavoidably leads to errors during the assembly process, which need to be corrected.

To be able to investigate the assembly process and the error-correction steps involved, a mixed-flow microreactor was coupled to the electrospray ion source. With this setup, reactants can be mixed directly in front of the ion source. Reaction times down to about one-half a second can be realized with this simple and easy-to-setup addition to the ion source.

On the basis of the knowledge of axle exchange rates of the individual simple pseudorotaxanes, the self-assembly and self-sorting steps involved in assembly formation have been investigated starting with a small four-component self-sorting system. The results obtained by using mass spectrometry to monitor the reactions parallel those obtained from NMR experiments and thus validate the mass spectrometric method applied. More complex self-sorting systems include sequence-specific [3]pseudorotaxanes with a ditopic axle and two monomeric crown ethers as well as [3]pseudorotaxanes consisting of a crown ether heterodimer and two monotopic axles. The mass spectrometric experiments provide interesting information on the major assembly pathways, which lead to the final, thermodynamic products. Control experiments provide more insight into the assembly mechanisms. They also demonstrate that the assembly pathways as well as the concentration of the intermediates depend much on the starting point chosen for the reaction. For the intermediate steps, but of course not for the final equilibrium, it matters whether the assembly begins with a mixture of the building blocks or whether preassembled reactants are involved.

Finally, two examples for multiply threaded pseudorotaxanes are presented. Although a large number of different assembly pathways can be imagined, quite clear-cut insight into the assembly steps can be obtained in both cases. On one hand, the use of an anthracene-stoppered axle reduces the potentially possible mechanisms significantly, because the anthracene does not allow any threading to occur on its side of the axle. On the other hand, the order of the threading rates leads to the accumulation of intermediates, when subsequent steps are slow. Both factors together clearly point to the operation of one particular major assembly pathway for the antiparallel assembly **12**-4H·4PF$_6$, while a number of equilibrating intermediates are found for the counterpart **13**-4H·4PF$_6$ bearing a parallel arrangement of the two axles.

Experimental Section

General Methods. Dibenzo-24-crown-8 (**C8**) was purchased from ACROS and used without further purification. Solvents were either employed as purchased or dried prior to use by usual laboratory methods. ^{1}H NMR spectra were recorded on Jeol Eclipse 500 MHz or Bruker Advance III 700 MHz NMR spectrometers. All chemical shifts are reported in ppm with residual solvents as the internal standards. The syntheses of benzo-21-crown-7 (**C7**), **1**-H·PF$_6$, **2**-H·PF$_6$, **3**-2H·2PF$_6$, **4**, **5**, and **6** have been reported earlier.[12]

ESI-FTICR-MS Experiments. The electrospray-ionization Fourier-transform ion-cyclotron-resonance (ESI-FTICR) mass spectrometric experiments were performed with a Varian/IonSpec QFT-7 FTICR mass spectrometer equipped with a superconducting 7 T magnet and a Micromass Z-spray ESI ion source utilizing a stainless steel capillary with a 0.65 mm inner diameter. The solutions of samples were introduced into the source with a syringe pump (Harvard Apparatus) at a flow rate of approximately 2.0 μL min^{-1}. Parameters were adjusted as follows: source temperature, 40 °C; temperature of desolvation gas, 40 °C; extractor cone, 10 V; capillary voltage was adjusted to minimize fragmentation and unspecific binding during ionization, 3000 V for **10**-2H·2PF$_6$ and the self-sorting system of **7**-H·PF$_6$/**8**-H·PF$_6$/**9**-H·PF$_6$, 3800 V for **11**-4H·4PF$_6$, **12**-2H·2PF$_6$, and **13**-4H·4PF$_6$; sample cone, adjusted between 10−60 V for maximum intensities; the detector's frequency was also adjusted to focus on the target *m*/*z* range. No nebulizer gas was used for the experiments. The ions were accumulated in the instrument's hexapole long enough to obtain useful signal-to-noise ratios. Next, the ions were introduced into the FTICR analyzer cell, which was operated at pressures below 10^{-9} mbar, and detected by a standard excitation and detection sequence. For each measurement, 20 scans were averaged to improve the signal-to-noise ratio.

Short time scales down to ca. 1 s can be achieved by using the mixed-flow microreactor described above. The PEEK mixing Tee microreactor, the necessary fittings, and capillaries were purchased from Scientific Instrument Services. The dead volume of the mixing Tee is as small as 4 μL. It contains a 5 μm PTFE filter, which enhances thorough mixing of the two solutions introduced into the microreactor chamber. Capillary sizes and diameters have been given in the main text. To introduce both solutions at the same speed, the instrument is equipped with a double syringe pump. The resulting mixture (250 μM in each component) is introduced into the ESI ion source through two sequential capillaries (part I (adjustable capillary), length, 6.3 cm; diameter, 125 μm; part II (fixed capillary inside the ion source), length, 16 cm; diameter, 75.0 μm). In this work, the flow rate was adjusted to achieve different reaction times. For example, 4 μL/min (2 μL/min for each syringe) corresponds to 22 s.

Acknowledgment. We thank Dr. Andreas Springer, Henrik D. F. Winkler, M.Sc., and Dipl.-Chem. Ralf W. Troff for help with the ESI-FTICR experiments and inspiring discussions, respectively. We gratefully acknowledge funding by the Deutsche Forschungsgemeinschaft (SFB 765) and the Fonds der Chemischen Industrie. Dedicated to Professor Jürgen Fuhrhop on the occasion of his 70th birthday.

Supporting Information Available: A series of ^{1}H NMR spectra recorded during the formation of **11**-2H·2PF$_6$ from **1**-H·PF$_6$, **2**-H·PF$_6$, and **4**; ^{1}H NMR and ESI-MS spectra of **15**-2H·2PF$_6$, **18b**-H·PF$_6$, **19**-H·PF$_6$, **20**-2H·2PF$_6$, a 1:2 mixture of **3**-2H·2PF$_6$ and **6**, and a 1:2:1 mixture of **1**-H·PF$_6$, **2**-H·PF$_6$, and **4**; and ^{1}H−^{1}H COSY spectra of **18b**-H·PF$_6$ and **20**-2H·2PF$_6$. This material is available free of charge via the Internet at http://pubs.acs.org.

JA9101369